Available online at www.sciencedirect.com

ScienceDirect

Ceramics International 40 (2014) 2343–2348

CERAMICS INTERNATIONAL

www.elsevier.com/locate/ceramint

The effects of citrate ion on morphology and photocatalytic activity of flower-like $Bi_2O_2CO_3$

Suqin Liu[a,b], Yangqin Tu[a], Gaopeng Dai[a,b,*]

[a]Department of Chemical Engineering and Food Science, Hubei University of Arts and Science, Xiangyang 441053, PR China
[b]Hubei Key Laboratory of Low Dimensional Optoelectronic Materials and Devices, Xiangyang 441053, PR China

Received 23 July 2013; accepted 1 August 2013
Available online 9 August 2013

Abstract

Flower-like $Bi_2O_2CO_3$ was synthesized in an aqueous solution containing bismuth nitrate, citric acid and urea. The as-prepared samples were characterized by X-ray diffraction, scanning electron microscopy, N_2 adsorption–desorption and UV-visible diffuse reflectance spectroscopy. The photocatalytic activity was evaluated by the photocatalytic degradation of methyl orange in an aqueous solution under Xe lamp irradiation. The effects of citrate ion on the morphology and photocatalytic activity were investigated. The results show that citrate ions facilitate the formation of hierarchical flower-like $Bi_2O_2CO_3$ microsphere. The amount of citric acid is an important parameter to control the morphology and size of $Bi_2O_2CO_3$ microsphere. The flower-like $Bi_2O_2CO_3$ exhibited an enhanced photocatalytic activity than $Bi_2O_2CO_3$ blocks. The highest photocatalytic performance can be achieved for the $Bi_2O_2CO_3$ microspheres synthesized in the solution with the $C_6H_8O_7/Bi(NO_3)_3$ M ratio of 2:1 due to the synergic effects of several factors, including its better crystallinity, larger surface area, stronger UV-visible absorption and unique hierarchical microsphere structure.

Keywords: Flower-like $Bi_2O_2CO_3$; Citrate ion; Photocatalytic; Morphology

1. Introduction

The optical and electrical properties and catalytic performance of materials strongly depend on their morphology and structure. Nanomaterials with controllable morphology, orientation, and dimensions have been extensively studied owing to their unique and promising properties [1–3]. In particular, three-dimensional (3D) hierarchical architectures which are assembled by nanoscaled building blocks have attracted considerable research interest because of their improved performances and successful applications in antibacterial agents, gas sensors, and photocatalysis [4–7]. For example, hierarchical TiO_2 spheres show high photocatalytic performance in photocatalytic decolorization of rhodamine B [8]. Flower-like ZnO exhibits excellent properties in photocatalytic degradation of rhodamine B [9]. Over the past few decades, many efforts have been devoted to fabricating 3D nano/microstructures and to exploring their unique morphology- or structure-dependent properties.

Recently, bismuth-containing nanostructures with 3D hierarchical architectures have stimulated extensive research interest, owing to their broad applications in the fields of electronics, biomedicine, and environmental science, such as Bi_2O_3 [10], Bi_2S_3 [11], Bi_2WO_6 [12], Bi_2MoO_6 [13], BiOBr [14] and $Bi_2O_2CO_3$ [15]. Among these compounds, bismuth subcarbonate ($Bi_2O_2CO_3$), possesses a typical Sillén phase, in which $Bi_2O_2^{2+}$ layers and CO_3^{2-} layers are intergrown with a plane of the CO_3^{2-} group orthogonal to the plane of the $Bi_2O_2^{2+}$ layer [16]. Very recently, it has been found to exhibit promising antibacterial performance and photocatalytic activity for the degradation of pollutants [17–22]. For example, Cao et al. synthesized persimmon-like $Bi_2O_2CO_3$ hierarchical structures with uniform size by a hydrothermal method, and it showed high photocatalytic efficiency in the degradation of RhB and eosin sodium salt under simulated solar irradiation [21]. Xie's group firstly synthesized $Bi_2O_2CO_3$ nanoflowers, nanosponges, and nanoplates by a simple hydrothermal process and further

*Corresponding author at: Department of Chemical engineering and Food Science, Hubei University of Arts and Science, Xiangyang 441053, PR China. Tel.: +867 103 592 609.
E-mail address: dgp2000@126.com (G. Dai).

0272-8842/$ - see front matter © 2013 Elsevier Ltd and Techna Group S.r.l. All rights reserved.
http://dx.doi.org/10.1016/j.ceramint.2013.08.004

investigated their visible-light driven photocatalytic activity [16]. N-doped $Bi_2O_2CO_3$ hierarchical microspheres were synthesized by a template-free hydrothermal method and exhibited excellent visible light photocatalytic activity [17]. Hierarchical $Bi_2O_2CO_3$ microspheres were synthesized using tri-sodium citrate as both the coordinating agent and carbon source and showed powerful visible-light photocatalytic activity [18]. Chen et al. developed a low-cost method for the synthesis of flower-like $Bi_2O_2CO_3$ in an aqueous medium with the assistance of cetyltrimethylammonium bromide [20].

Herein, we synthesized flower-like $Bi_2O_2CO_3$ by hydrothermal treatment of bismuth nitrate, citric acid and urea in water, and then investigated the effects of citrate ion on the morphology and photocatalytic activity of $Bi_2O_2CO_3$.

2. Experimental

2.1. Sample preparation

All reagents used in this study were of analytical grade and were purchased from Shanghai Chemical Reagent Factory of China without further purification. Distilled water was used in all experiments. In a typical fabrication, 4.85 g of $Bi(NO_3)_3 \cdot 5H_2O$ and different amounts of $C_6H_8O_7 \cdot H_2O$ were mixed into 90 mL of distilled water under stirring at room temperature. Subsequently, the solution was subjected to an ultrasonic process (1 h) and vigorous stirring (3 h). Then, 1.8 g of urea was added into the above solution. After another 30 min stirring, the solution was transferred into a 150 mL Teflon-sealed autoclave and maintained at 180 °C for 12 h. After hydrothermal reaction, the precipitate was collected, washed with ethanol and distilled water for three times, and then dried in an oven at 100 °C for 6 h. The samples synthesized with different amounts (0, 2.1, 4.2, 6.3 and 8.4 g) of $C_6H_8O_7 \cdot H_2O$ were labeled as BC-0, BC-1, BC-2, BC-3 and BC-4, respectively. The detailed experiment parameters are listed in Table 1.

2.2. Characterization

The X-ray diffraction (XRD) patterns, which were used to characterize the crystalline phases, were carried out on an X-ray diffractometer (D/MAX-RB, Rigaku, Japan) using Cu Ka radiation at a scan rate of 0.05° $2\theta\ s^{-1}$. The accelerating voltage and the applied current were 40 kV and 80 mA, respectively. The morphology observation was performed on an S-4800 field emission scanning electron microscopy (FESEM, Hitachi, Japan), analysis was performed at accelerating voltage of 10 kV. The Brunauer–Emmett–Teller (BET) surface area (S BET) of the powders was evaluated on the basis of nitrogen adsorption isotherms measured on a Micromeritics ASAP 2020 adsorption apparatus (USA). All samples were degassed at 160 °C prior to nitrogen adsorption measurements. The BET surface area was determined by a multipoint BET method using the adsorption data in the relative pressure (P/P_0) range of 0.05–0.3. The UV-visible diffuse reflectance spectra of the materials studied were obtained for the dry-pressed film samples using a UV-visible spectrophotometer (UV-2550, Shimadzu, Japan). $BaSO_4$ was used as a reflectance standard in the UV-visible diffuse reflectance experiments.

2.3. Evaluation of photocatalytic activity

The photocatalytic activity of the samples was evaluated by the photocatalytic decolorization of methyl orange (MO) aqueous solution at ambient temperature. In detail, 0.1 g of the as-prepared catalyst powders was dispersed in a 25 mL of 4×10^{-5} M MO aqueous solution in a 7.0 cm culture dish. Prior to illumination, the resulting mixture was allowed to reach the adsorption–desorption equilibrium. A 200 W xenon lamp positioned 25 cm above the dish was used as light source to trigger the photocatalytic reaction. The concentration of MO was determined by an UV-visible spectrophotometer (UV-2550, Shimadzu, Japan).

3. Results and discussion

3.1. Phase structures

The compositions and structures of the as-prepared products were characterized by powder X-ray diffraction and electron microscopy. Fig. 1 shows the XRD patterns, and the tetragonal phase of $Bi_2O_2CO_3$ (JCPDS no. 41-1488) was identified in all samples. Some impure diffraction peaks in 25.7°, 28.6°, 31.3° and 46° can be observed obviously in BC-0 sample, suggesting that other impurities exist in the sample. In contrast, no other crystalline impurities were detected in all samples synthesized with citric acid. A detailed analysis of the XRD patterns shows that the XRD peak intensities of samples prepared with citric acid are weaker than the sample synthesized without citric acid, and the peak widths are wider than that of BC-0,

Table 1
Experimental conditions for the synthesis of $Bi_2O_2CO_3$.

Sample	$C_6H_8O_7/Bi(NO_3)_3$ M ratio	$Urea/Bi(NO_3)_3$ M ratio	Morphology
BC-0	0	3	Block
BC-1	1	3	Microsphere
BC-2	2	3	Microsphere
BC-3	3	3	Microsphere
BC-4	4	3	Microsphere

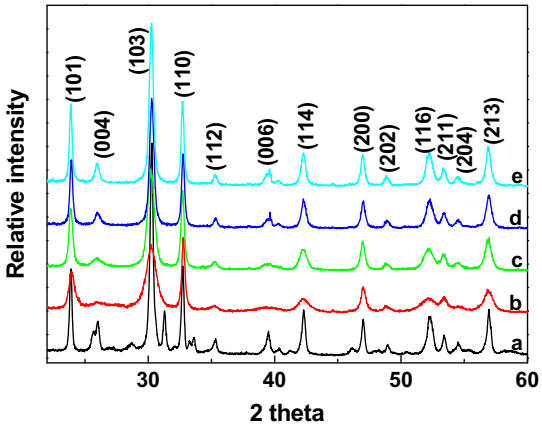

Fig. 1. XRD patterns of BC-0 (a), BC-1 (b), BC-2 (c), BC-3 (d) and BC-4 (e) samples.

implying the formation of weaker $Bi_2O_2CO_3$ crystallites in the samples synthesized with citric acid. Further observation shows that the XRD peak intensities increase with the increasing amount of citric acid in the samples synthesized with citric acid. The results suggest that citrate ion plays a key role in the synthesis and crystal growth of pure $Bi_2O_2CO_3$. Without citrate ion, $Bi_2O_2CO_3$ formation occurs as follows.

$$NH_2CONH_2+H_2O \rightarrow CO_3^{2-}+NH^{4+} \quad (1)$$

$$Bi(NO3)_3+H_2O \rightarrow BiONO_3+H^{+}+2NO_3^{-} \quad (2)$$

$$CO_3^{2-}+BiONO_3 \rightarrow Bi_2O_2CO_3+NO_3^{-} \quad (3)$$

After the addition of citric acid, $Bi(NO_3)_3 \cdot 5H_2O$ can react with $C_6H_8O_7 \cdot H_2O$ to form bismuth citrate (Eq. 4) [16], which would control the releasing of Bi^{3+}. With the hydrothermal

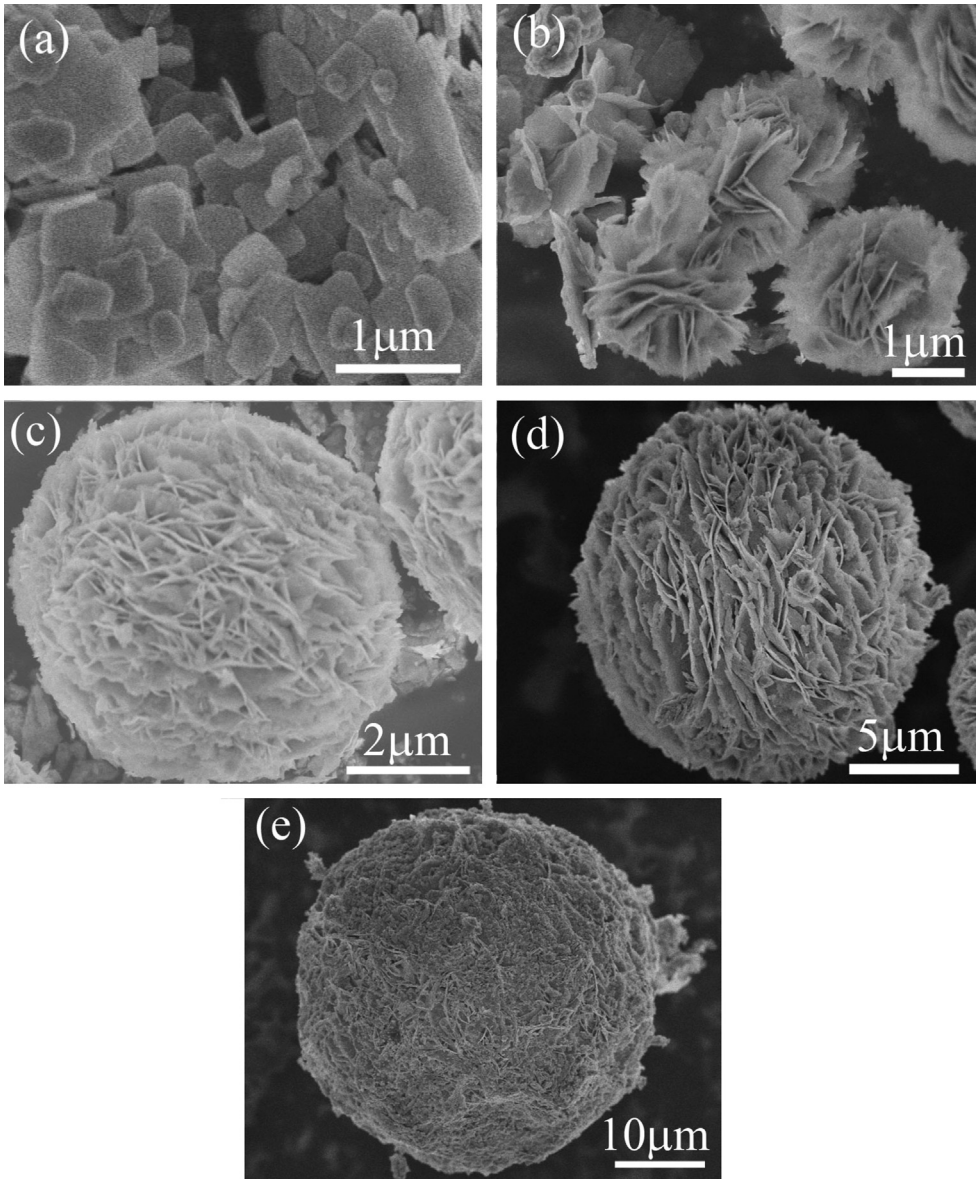

Fig. 2. SEM images of BC-0 (a), BC-1 (b), BC-2 (c), BC-3 (d) and BC-4 (e) samples.

temperature increasing, bismuth citrate was gradually decomposed to release Bi^{3+} and CO_3^{2-}, and then the former reacted with H_2O to generate BiO^+. Subsequently, the CO_3^{2-}, which was generated from NH_2CONH_2 and $C_6H_5O_7Bi$, reacted with BiO^+ to form $Bi_2O_2CO_3$, the possible reaction mechanism is shown below.

$$Bi^{3+}+C_6H_5O_7{}^{3-}\rightleftharpoons C_6H_5O_7Bi \quad (4)$$

$$C_6H_5O_7Bi+H_2O\rightarrow BiO^+ + CO_3{}^{2-}+H^+ \quad (5)$$

$$BiO^+ + CO_3{}^{2-}\rightarrow Bi_2O_2CO_3 \quad (6)$$

Based on the above reaction mechanism, citrate ion may play an important role in controlling the releasing of BiO^+ and the formation rate of $Bi_2O_2CO_3$. In the system containing citric acid, the slow release of BiO^+ from $C_6H_5O_7Bi$ lead to the slow formation of $Bi_2O_2CO_3$, and then the slow crystal growth of $Bi_2O_2CO_3$. On the other hand, with the increase of citric acid amount, the concentration of CO_3^{2-} increases, resulting in the increase of formation rate of $Bi_2O_2CO_3$ and the fast crystal growth of $Bi_2O_2CO_3$. Therefore, it is not surprising that the $Bi_2O_2CO_3$ crystallites in the samples synthesized with citric acid were weaker than that in the sample without citric acid, and the XRD peaks intensities increase with the increasing amount of citric acid in the samples synthesized with citric acid.

3.2. Morphologies

The morphologies of the as-prepared $Bi_2O_2CO_3$ samples are displayed in Fig. 2. It can be seen that the flower-like microspheres consisted of thin flakes were synthesized in solution containing citric acid, and the microshpere size increases with the increasing citric acid amount. However, only blocks with size about 500 nm–1 μm were obtained without citric acid. The results indicated that citrate ion plays a decisive role in the formation and growth of flower-like $Bi_2O_2CO_3$ microspheres.

It has been reported that citrate can serve as a shape modifier and controller, which may bind to certain crystal faces of the particles through its COO– and –OH functions [23]. Citrate ions can also be strongly absorbed on the mineral surfaces, leading to the formation of nanosheets with thin thickness [24,25]. According to the crystal structure of $Bi_2O_2CO_3$, the $Bi_2O_2{}^{2+}$ layers and CO_3^{2-} layers are intergrown with the plane of the CO_3^{2-} group orthogonal to the plane of the $Bi_2O_2{}^{2+}$ layer. Such an internal layered structure would guide the lower growth rate along a certain axis to form a 2D nanosheet morphology [26,27]. Without citric acid, a great deal of $Bi_2O_2CO_3$ nanosheets were formed quickly, followed by a rapid aggregation to form blocks due to no absorption of citrate ion to decrease the surface energy. However, in the system containing citric acid, nanosheets formed slowly, and then aggregate into large particles with separated nanosheets due to the absorption of citrate ions on the nanosheets surfaces. Finally, these particles spontaneously initiate a dissolution–recrystallization process, followed by Ostwald ripening. With reaction time, the flower-like $Bi_2O_2CO_3$ microspheres with thin flakes were formed [27]. With the increasing citrate ion amount, the formation rate of $Bi_2O_2CO_3$ nanosheets increases, and subsequently they aggregate into larger particles, hence, enhancing the microsphere size.

3.3. BET surface

It is widely accepted that photocatalysts with higher specific surface area and porous structures are beneficial to the enhancement of photocatalytic performance, due to more surface active sites for the adsorption of reactant molecules, ease transportation of reactant molecules and products through the interconnected porous networks, and enhanced harvesting of exciting light by multiple scattering within the porous framework [28]. Herein, the effects of citrate ion on the pore structure and BET surface areas of $Bi_2O_2CO_3$ samples are investigated by the nitrogen sorption measurement. The surface area of BC-0 sample is too small to be detected. Fig. 3 shows the nitrogen adsorption–desorption isotherms at 77 K for the $Bi_2O_2CO_3$ samples synthesized in the solutions containing citric acid. These isotherms have hysteresis loops characteristic for mesoporous solids (2–50 nm), which classify them as type IV according to Brunauer–Deming–Deming–Teller (BDDT) classification [29]. Note that the adsorption branches of these isotherms resemblance type II, indicating the presence of some macropores. The hysteresis loops can be categorized as type H3 associated with slit-like mesopores formed between $Bi_2O_2CO_3$ nanosheets.

The presence of citrate ion in the synthesis mixture has a significant influence on the nitrogen adsorption–desorption isotherms. With the increasing citric acid amount, the surface area decreases, and the hysteresis loops are gradually shifted in direction of higher relative pressures, indicating that mesopores in samples is significantly larger and larger due to the gradually increasing size of $Bi_2O_2CO_3$ nanosheets (Fig. 2), which are the primary building units. The BET surface areas of BC-1, BC-2, BC-3 and BC-4 are 54.3, 20.2, 14.9 and 8.1 m^2/g, respectively.

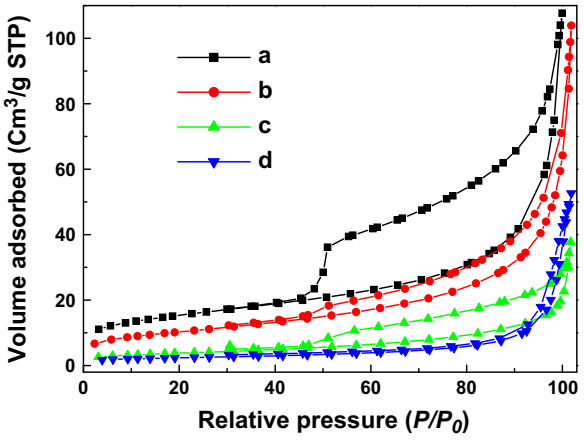

Fig. 3. Nitrogen adsorption–desorption isotherms of BC-1 (a), BC-2 (b), BC-3 (c) and BC-4 (d) samples.

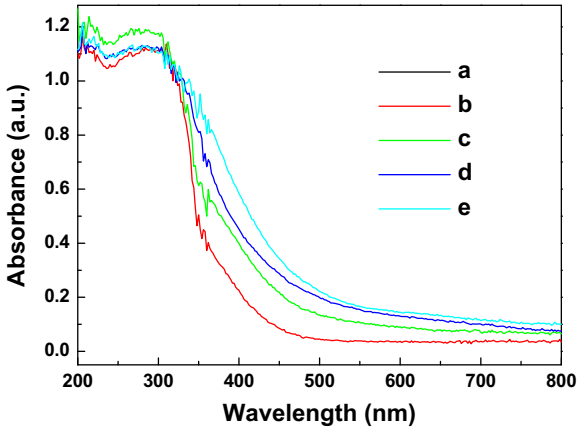

Fig. 4. UV–vis diffuse reflectance spectra of BC-0 (a), BC-1 (b), BC-2 (c), BC-3 (d) and BC-4 (e) samples.

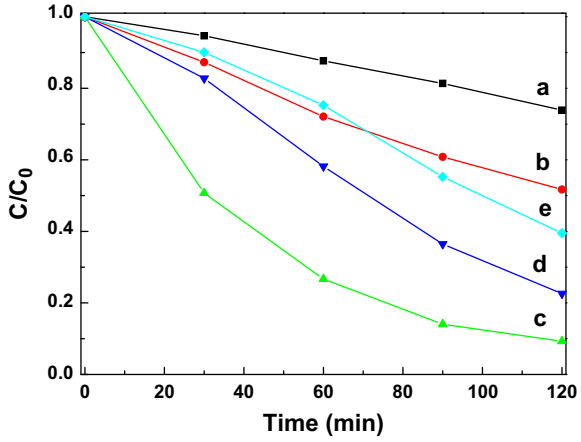

Fig. 5. Comparison of photocatalytic activity of samples BC-0 (a), BC-1 (b), BC-2 (c), BC-3 (d) and BC-4 (e) for the photocatalytic decomposition of MO in water.

3.4. UV−vis absorption properties

Fig. 4 shows the UV−vis diffuse absorption spectra for $Bi_2O_2CO_3$ samples. As for the $Bi_2O_2CO_3$ blocks (BC-0), only the band gap absorption with a steep absorption edge at the UV region can be observed. In contrast, the flower-like samples exhibit an enhanced absorption in the whole light range, especially in the visible-light region. Moreover, the absorption edge at about 390 nm shows an obvious red shift. The results are in a good agreement with the previous literature [27]. It is reported that morphologies greatly affect the optical absorption and bandgap energy of the $Bi_2O_2CO_3$ samples [27]. $Bi_2O_2CO_3$ with hierarchical flower-like superstructure has a red shift in the bandgap transition compared with $Bi_2O_2CO_3$ nanosheets structures. The above optical properties would facilitate the photocatalytic decomposition of organic contaminants.

3.5. Photocatalytic activity

The photocatalytic activities of the $Bi_2O_2CO_3$ samples were evaluated by photocatalytic degradation decolorization of MO aqueous solution under Xe lamp irradiation. Fig. 5 shows the comparison of photocatalytic activities of different samples. Only 36.2% of MO dye molecules are decomposed over the $Bi_2O_2CO_3$ blocks after irradiation for 40 min. However, MO dyes are greatly bleached in the presence of the $Bi_2O_2CO_3$ flower-like microspheres and the photodegradation efficiency reaches 48.3%, 90.8, 77.5 and 60.5 over the samples BC-1, BC-2, BC-3 and BC-4, respectively. BC-2 displays a highest photocatalytic activity.

The high activity of BC-2 sample can be attributed to the synergetic effects of several factors. First, the better crystallinity of BC-2 sample (Fig. 1) enhances the generation and migration of photogenerated electron/hole pairs in the bulk and surface of photocatalyst [30], and thus improves its photocatalytic activity. Second, the larger surface area of BC-2 sample cannot only offer more active sites for photocatalytic reactions but also effectively promote the separation efficiency of the photocatalytic reaction [27–31]. Third, the stronger intensity of UV-visible absorption of flower-like $Bi_2O_2CO_3$ microsphere implies that more photogenerated electrons and holes can participate in the photocatalytic reaction, resulting in higher photocatalytic activity [32]. Fourth, the $Bi_2O_2CO_3$ microspheres with unique porous thinner 2D nanosheets could provide more efficient transport channels for the diffusion of the reactants and products in the photocatalytic process, facilitating its superior photocatalytic activity [27].

4. Conclusions

Flower-like $Bi_2O_2CO_3$ was synthesized via hydrothermal treatment of aqueous solution of bismuth nitrate, citric acid and urea. The presence of citrate ion plays a determined role in the formation of flower-like $Bi_2O_2CO_3$ microspheres with thin flakes. With the increasing amount of citrate ion, the size of $Bi_2O_2CO_3$ microspheres increases. The $Bi_2O_2CO_3$ microspheres synthesized in the solution with the $C_6H_8O_7$/Bi$(NO_3)_3$ M ratio of 2:1 show the highest photocatalytic activity. The significant improvement in the photocatalytic performance could be attributed to the better crystallinity, larger surface area, stronger UV–visible absorption and unique hierarchical microsphere structure.

Acknowledgments

This work was financially supported by the Natural Science Foundation of Hubei Province (2012FFB01903), the Research Program of Hubei Province Department of Education (Q20132608 and Q20122507) and Xiangyang Science and Technology Bureau.

References

[1] Y. Xia, P. Yang, Y. Sun, Y. Wu, B. Mayers, B. Gates, Y. Yin, F. Kim, H. Yan, One-dimensional nanostructures: synthesis, characterization, and applications, Advanced Materials 15 (2003) 353–389.

[2] J. Xiong, G. Cheng, Z. Lu, J. Tang, X. Yu, R. Chen, BiOCOOH hierarchical nanostructures: Shape-controlled solvothermal synthesis and photocatalytic degradation performances, Crystal Engineering Communications 13 (2011) 2381–2390.

[3] J.G. Yu, W. Liu, H.G. Yu, A One-Pot, Approach to hierarchically nanoporous titania hollow microspheres with high photocatalytic activity, Crystal Growth and Design 8 (2008) 930–934.
[4] X.X. Yu, J.G. Yu, B. Cheng, M. Jaroniec, Synthesis of hierarchical flower-like AlOOH and TiO_2/AlOOH superstructures and their enhanced photocatalytic properties, Journal of Physical Chemistry C 113 (2009) 17527–17535.
[5] X.H. Yan, Q.X. Gao, J.L. Qin, X.F. Yang, Y. Li, H. Tang, Morphology-controlled synthesis of Ag_3PO_4 microcubes with enhanced visible-light-driven photocatalytic activity, Ceramics International. http://dx.doi.org/10.1016/j.ceramint.2013.04.044.
[6] Z. Chen, M.H. Cao, C.W. Hu, Novel Zn_2SnO_4 hierarchical nanostructures and their gas sensing properties toward ethanol, Journal of Physical Chemistry C 115 (2011) 5522–5529.
[7] H. Li, J. Zhang, X.F. Chen, G.F. Pan, Y.N. Huo, Ionic-liquid-assisted growth of flower-like TiO_2 film on Ti substrate with high photocatalytic activity, Journal of Molecular Catalysis A: Chemical 373 (2013) 12–17.
[8] G.G. Tang, S.S. Liu, H. Tang, D. Zhang, C.S. Li, X.F. Yang, Template-assisted hydrothermal synthesis and photocatalytic activity of novel TiO_2 hollow nanostructures, Ceramics International 39 (2013) 4969–4974.
[9] B.X. Li, Y.F. Wang, Facile synthesis and enhanced photocatalytic performance of flower-like ZnO hierarchical microstructures, Journal of Physical Chemistry C 114 (2010) 890–896.
[10] L. Zhang, Y. Hashimoto, T. Taishi, I. Nakamura, Q.Q. Ni, Fabrication of flower-shaped Bi_2O_3 superstructure by a facile template-free process, Applied Surface Science 257 (2011) 6577–6582.
[11] H.Y. Zhou, S.L. Xiong, L.Z. Wei, B.J. Xi, Y.C. Zhu, Y.T. Qian, Acetylacetone-directed Controllable synthesis of Bi_2S_3 nanostructures with tunable morphology, Crystal Growth and Design 9 (2009) 3862–3867.
[12] P. Dumrongrojthanath, T. Thongtem, A. Phuruangrat, S. Thongtem, Hydrothermal synthesis of Bi_2WO_6 hierarchical flowers with their photonic and photocatalytic properties, Superlattices and Microstructures 54 (2013) 71–77.
[13] Y.S. Xu, Z.J. Zhang, W.D. Zhang, Facile preparation of heterostructured Bi_2O_3/Bi_2MoO_6 hollow microspheres with enhanced visible-light-driven photocatalytic and antimicrobial activity, Materials Research Bulletin 48 (2013) 1420–1427.
[14] J. Zhang, F.J. Shi, J. Lin, D.F. Chen, J.M. Gao, Z.X. Huang, X.X. Ding, C.C. Tang, Self-assembled 3-D architectures of BiOBr as a visible light-driven photocatalyst, Chemistry of Materials 20 (2008) 2937–2941.
[15] R. Chen, G. Cheng, M.H. So, J. Wu, Z. Lu, C.-M. Che, H. Sun, Bismuth subcarbonate nanoparticles fabricated by water-in-oil microemulsion-assisted hydrothermal process exhibit anti-*Helicobacter pylori* properties, Materials Research Bulletin 45 (2010) 654–658.
[16] Y. Zheng, F. Duan, M.Q. Chen, Y. Xie, Synthetic $Bi_2O_2CO_3$ nanostructures: novel photocatalyst with controlled special surface exposed, Journal of Molecular Catalysis A: Chemical 317 (2010) 34–40.
[17] F. Dong, Y.J. Sun, M. Fu, W.K. Ho, S.C. Lee, Z.B. Wu, Novel in situ N-doped $(BiO)_2CO_3$ hierarchical microspheres self-assembled by nanosheets as efficient and durable visible light driven photocatalyst, Langmuir 28 (2012) 766–773.
[18] T.Y. Zhao, J.T. Zai, M. Xu, Q. Zou, Y.Z. Su, K.X. Wang, X.F. Qian, Hierarchical $Bi_2O_2CO_3$ microspheres with improved visible-light-driven photocatalytic activity, Crystal Engineering Communications 13 (2011) 4010–4017.
[19] P. Madhusudan, J.G. Yu, W.G. Wang, B. Chenga, G. Liu, Facile synthesis of novel hierarchical graphene–$Bi_2O_2CO_3$ composites with enhanced photocatalytic performance under visible light, Dalton Transactions 41 (2012) 14345–14353.
[20] L. Chen, R. Huang, S.F. Yin, S.L. Luo, C.T. Au, Flower-like $Bi_2O_2CO_3$: facile synthesis and their photocatalytic application in treatment of dye-containing wastewater, Chemical Engineering Journal 193–194 (2012) 123–130.
[21] X.F. Cao, L. Zhang, X.T. Chen, Z.L. Xue, Persimmon-like $(BiO)_2CO_3$ microstructures: hydrothermal preparation, photocatalytic properties and their conversion into Bi_2S_3, Crystal Engineering Communications 13 (2011) 1939–1975.
[22] Y.Y. Liu, Z.Y. Wang, B.B. Huang, K.S. Yang, X.Y. Zhang, X.Y. Qin, Y. Dai, Preparation, electronic structure, and photocatalytic properties of $Bi_2O_2CO_3$ nanosheet, Applied Surface Science 257 (2010) 172–175.
[23] M. Hu, J.S. Jiang, X.D. Li, Surfactant-assisted hydrothermal synthesis of dendritic magnetite microcrystals, Crystal Growth and Design 9 (2009) 820–824.
[24] Z.R.R. Tian, J.A. Voigt, J. Liu, B. McKenzie, M.J. McDermott, M. A. Rodriguez, H. Konishi, H.F. Xu, Complex and oriented ZnO nanostructures, Nature Materials 2 (2003) 821–826.
[25] J.H. Kim, D. Andeen, F.F. Lange, Hydrothermal growth of periodic, single-crystal ZnO microrods and microtunnels, Advanced Materials 18 (2006) 2453–2457.
[26] C.Z. Wu, Y. Xie, Controlling phase and morphology of inorganic nanostructures originated from the internal crystal structure, Chemical Communications (2009) 5943–5957.
[27] P. Madhusudan, J. Zhang, B. Cheng, G. Liu, Photocatalytic degradation of organic dyes with hierarchical $Bi_2O_2CO_3$ microstructures under visible-light, Crystal Engineering Communications 15 (2013) 231–240.
[28] J.G. Yu, S.W. Liu, H.G. Yu, Microstructures and photoactivity of mesoporous anatase hollow microspheres fabricated by fluoride-mediated self-transformation, Journal of Catalysis 249 (2007) 59–66.
[29] K.S.W. Sing, D.H. Everett, R.A.W. Haul, L. Moscou, R.A. Pierotti, J. Rouquerol, T. Siemieniewska, Reporting physisorption data for gas/solid systems with special reference to the determination of surface area and porosity, Pure and Applied Chemistry Chimie Pure et Appliquée 57 (1985) 603–619.
[30] H. Zhang, J.F. Banfield, Thermodynamic analysis of phase stability of nanocrystalline titania, Journal of Materials Chemistry 8 (1998) 2073–2076.
[31] J. Tang, Z. Zou, J. Ye, Efficient photocatalytic decomposition of organic contaminants over $CaBi_2O_4$ under visible-light irradiation, Angewandte Chemie International Edition 43 (2004) 4463–4466.
[32] J.C. Yu, J.G. Yu, W.K. Ho, Z.T. Jiang, L.Z. Zhang, Effects of F-doping on the photocatalytic activity and microstructures of nanocrystalline TiO_2 powders, Chemistry of Materials 14 (2002) 3808–3816.